Detecting super-thin clouds with polarized sunlight

Wenbo Sun[1,2], Gorden Videen[3,4], and Michael I. Mishchenko[5]

[1]Science Systems and Applications Inc., Hampton, Virginia, USA, [2]NASA Langley Research Center, Hampton, Virginia, USA, [3]Space Science Institute, Boulder, Colorado, USA, [4]Army Research Laboratory, Adelphi, Maryland, USA, [5]NASA Goddard Institute for Space Studies, New York, New York, USA

Abstract We report a novel method for detecting cloud particles in the atmosphere. Solar radiation backscattered from clouds is studied with both satellite data and a radiative transfer model. A distinct feature is found in the angle of linear polarization of solar radiation that is backscattered from clouds. The dominant backscattered electric field from the clear-sky Earth-atmosphere system is nearly parallel to the Earth surface. However, when clouds are present, this electric field can rotate significantly away from the parallel direction. Model results demonstrate that this polarization feature can be used to detect super-thin cirrus clouds having an optical depth of only ~0.06 and super-thin liquid water clouds having an optical depth of only ~0.01. Such clouds are too thin to be sensed using any current passive satellite instruments.

Super-thin cirrus clouds with optical depths smaller than ~0.3 exist globally [*McFarquhar et al.*, 2000; *Sun et al.*, 2011b]. These clouds are important to the radiation energy balance of the Earth [*Sassen and Benson*, 2001; *Sun et al.*, 2011b]. They also can affect the remote sensing of aerosols [*Sun et al.*, 2011b], surface temperature [*Sun et al.*, 2011a], and atmospheric gases [*Christi and Stephens*, 2004]. For example, the aerosol optical depth (AOD) from NASA's Moderate Resolution Imaging Spectroradiometer (MODIS) data could be overestimated by ~100% when these clouds exist [*Sun et al.*, 2011b]. Failing to detect these clouds, the sea surface temperature (SST) retrieved from NASA's Atmospheric Infrared Sounder (AIRS) satellite data is ~5 K lower at tropical and midlatitude regions, where occurrence frequency of these clouds is high [*Sun et al.*, 2011a]. Climate models must incorporate these clouds correctly in order to account for the Earth's radiation energy budget. To intercalibrate other satellite sensors with NASA's future Climate Absolute Radiance and Refractivity Observatory (CLARREO) measurements [*Wielicki et al.*, 2013], knowledge on these clouds is also important for correcting those sensors' measurement errors due to light's polarization [*Sun and Lukashin*, 2013].

Due to uncertainties in surface reflectance, the transparent super-thin clouds generally cannot be detected by satellite imagers, like the MODIS and the Advanced Very High Resolution Radiometer that only measure the total radiance of the reflected solar light [*Ackerman et al.*, 2008]. The resulting data products of many satellite and ground measurements are biased by these undetected clouds [*Sun et al.*, 2011a, 2011b; *Omar et al.*, 2013]. Using a strong water vapor absorption channel such as the 1.38 μm radiance to exclude the surface and low-layer effects can be effective on high cirrus [*Gao and Kaufman*, 1995] but may encounter difficulties for atmospheres with low water vapor [*Ackerman et al.*, 1998]. The reliability of this method is also questionable if the clouds' optical depth is smaller than ~0.5, when their backscattered intensity is low [*Roskovensky and Liou*, 2003]. In addition, super-thin clouds may also exist in the lower layers of the atmosphere where there is ample water vapor. The sensitivity of the 1.38 μm channel is weak in this region, hampering detection capabilities. NOAA's polar orbiting High Resolution Infrared Radiation Sounder multispectral infrared data are usually used with the CO_2-slicing method for detecting thin cirrus clouds [*Wylie et al.*, 1995; *Wylie and Menzel*, 1999]. However, for super-thin clouds, this requires the radiance of their background atmosphere and surface to be very close to that of the reference clear-sky environment, which can be difficult as the terrestrial background changes on spatial and temporal scales. In addition, this method is problematic when the difference between clear-sky and cloudy radiance for a spectral band is less than the instrument noise [*Wylie and Menzel*, 1999], as for super-thin clouds.

Currently, the Cloud-Aerosol Lidar and Infrared Pathfinder Satellite Observation lidar [*Winker et al.*, 2007] is the only instrument in orbit that can detect super-thin clouds. However, long-term global surveys of super-thin clouds using space-borne lidar are limited by the large operational cost and narrow field of view of this active instrument. In this letter, we report a novel method for using passive polarimetric instruments such as
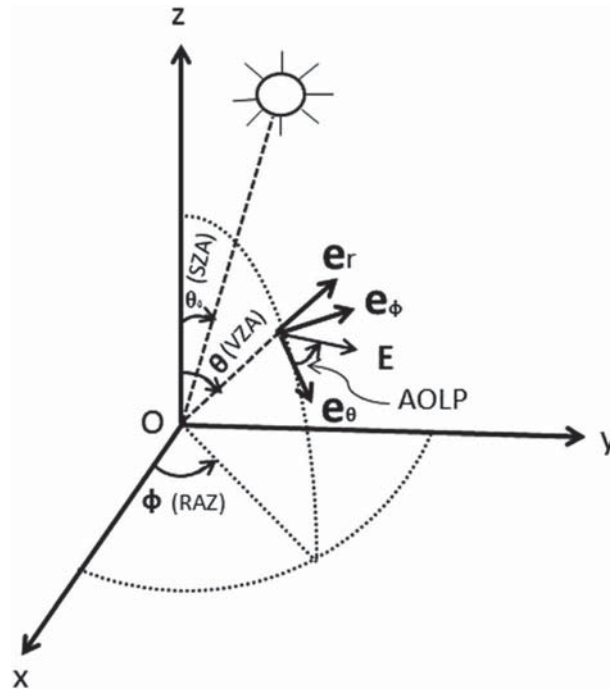
Figure 1. The geometry of the system showing the scattered light from a surface located in the *x-y* plane. The Sun is located on the principal plane (*xoz*) and over the negative *x* axis (i.e., the solar azimuth angle is 180°). The direction of the reflected light is specified by the unit vector $\mathbf{e}_r$, and θ and ϕ denote the viewing zenith angle (VZA) and relative azimuth angle (RAZ), respectively. In the local right-handed orthonormal coordinate system $\mathbf{e}_r = \mathbf{e}_\theta \times \mathbf{e}_\phi$, where $\mathbf{e}_\theta$ lies in the meridian plane of the reflected light beam. The AOLP of the reflected beam in the direction of $\mathbf{e}_r$ is the angle between the local meridian line and the electric vector **E** of the linearly polarized light, counted anticlockwise when viewing in the reverse direction of the reflected beam. The electric field **E** of the linearly polarized part of the reflected light oscillates in the plane of $\mathbf{e}_\theta$ and $\mathbf{e}_\phi$.

the aerosol polarimetry sensor that was a part of NASA's Glory mission [*Mishchenko et al.*, 2007] to detect super-thin clouds.

A space-borne polarimetric instrument can measure the Stokes parameters *I*, *Q*, *U*, and *V* of the scattered light [*Mishchenko et al.*, 2007]. Since the circularly polarized component of radiance reflected by the ocean–atmosphere system is negligible ($V \approx 0$), the degree of polarization (DOP) and angle of linear polarization (AOLP) can be defined in terms of Stokes parameters as [*Sun and Lukashin*, 2013]

$$\mathrm{DOP} = \frac{\sqrt{Q^2 + U^2}}{I},$$ (1)

and

$$\mathrm{AOLP} = \frac{1}{2}\tan^{-1}\left(\frac{U}{Q}\right) + \alpha_0,$$ (2)

where $\alpha_0 = 0°$ if $Q > 0$ and $U \geq 0$; $\alpha_0 = 180°$ if $Q > 0$ and $U < 0$; and $\alpha_0 = 90°$ if $Q \leq 0$. In a right-handed Cartesian coordinate system, as shown in Figure 1, the AOLP of the reflected light is the angle between the local meridian line in the direction of $\mathbf{e}_\theta$ and the electric vector **E** of the linearly polarized part of the reflected light, measured anticlockwise when viewed in the reverse direction of the reflected radiance [*Sun and Lukashin*, 2013]. The electric field **E** of the linearly polarized part of the reflected light oscillates in the plane of $\mathbf{e}_\theta$ and $\mathbf{e}_\phi$ in Figure 1.

Natural solar radiation can be polarized by surface reflections as well as by scattering from atmospheric molecules and particles. When sunlight propagates through the clear atmosphere and is scattered back toward the Sun, the resulting signal is nearly unpolarized when the solar zenith angle (SZA) is not larger than ~40° [*Sun and Lukashin*, 2013]. The residual polarization in this direction is due to asymmetries in the system, due for instance to preferentially oriented ocean waves or nonzero angles between incidence and observation. By considering a longer solar wavelength, such as 670 nm, the contribution of molecular scattering is reduced. Moreover, unlike total radiance *I*, the DOP and AOLP are insensitive to surface roughness and
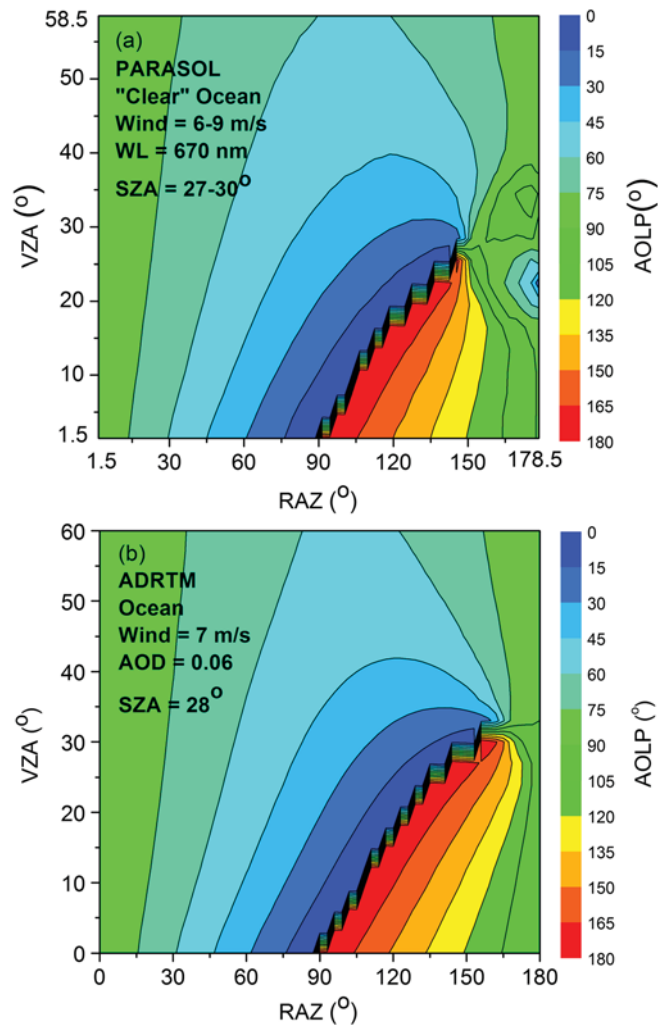
Figure 2. The AOLP at 670 nm as a function of VZA and RAZ from (a) the mean of 24 day PARASOL measurements for clear-sky oceans identified by the PARASOL product, and (b) the ADRTM for clear-sky oceans. The 24 days of PARASOL data are taken from the first 2 days of each month across 2006. Data are binned in SZA from 27° to 30° and in wind speed from 6 m/s to 9 m/s, and averaged in 3° bins in VZA and RAZ. In the modeling, the SZA is 28°, the ocean wind speed is 7 m/s, the sea-salt AOD is 0.06, and the U.S. standard atmosphere is used.

absorption by atmospheric water vapor and other gases [*Sun and Lukashin*, 2013], which makes the polarization measurement robust in different environmental conditions, even when the detected components are within the lower layers of the atmosphere. In brief, remote sensing atmospheric particulates using polarization measurements in the backscattering region can minimize surface, molecule, and absorbing gas interferences, thus increasing the sensitivity to atmospheric particulates, like super-thin clouds.

Because of to the variations in surface reflections and atmospheric profiles, using total reflection intensity to detect super-thin clouds is generally difficult. Also, although thin clouds can cause changes in the degree of polarization (DOP) of the reflected light [*Sun and Lukashin*, 2013], the dynamic range of the DOP change is mostly insufficient to unambiguously identify super-thin clouds if the background polarized reflection is uncertain. However, another fundamental characteristics of light is its angle of linear polarization (AOLP). Figure 2 shows the AOLPs at a wavelength $\lambda = 670$ nm (Figure 2a) taken from the mean of 24 day measurements for clear-sky oceans from the Polarization and Anisotropy of Reflectances for Atmospheric Science coupled with Observations from a Lidar (PARASOL) product [*Deschamps et al.*, 1994], and (Figure 2b) calculated using the adding-doubling radiative transfer model (ADRTM) [*Sun and Lukashin*, 2013] for clear-sky oceans. The 24 days of PARASOL data are taken from the first 2 days of each month across 2006 and collected in a SZA bin of 27–30° and a wind speed bin of 6–9 m/s, and averaged in 3° bins in viewing zenith angle (VZA) and relative azimuth angle (RAZ). In the modeling, the
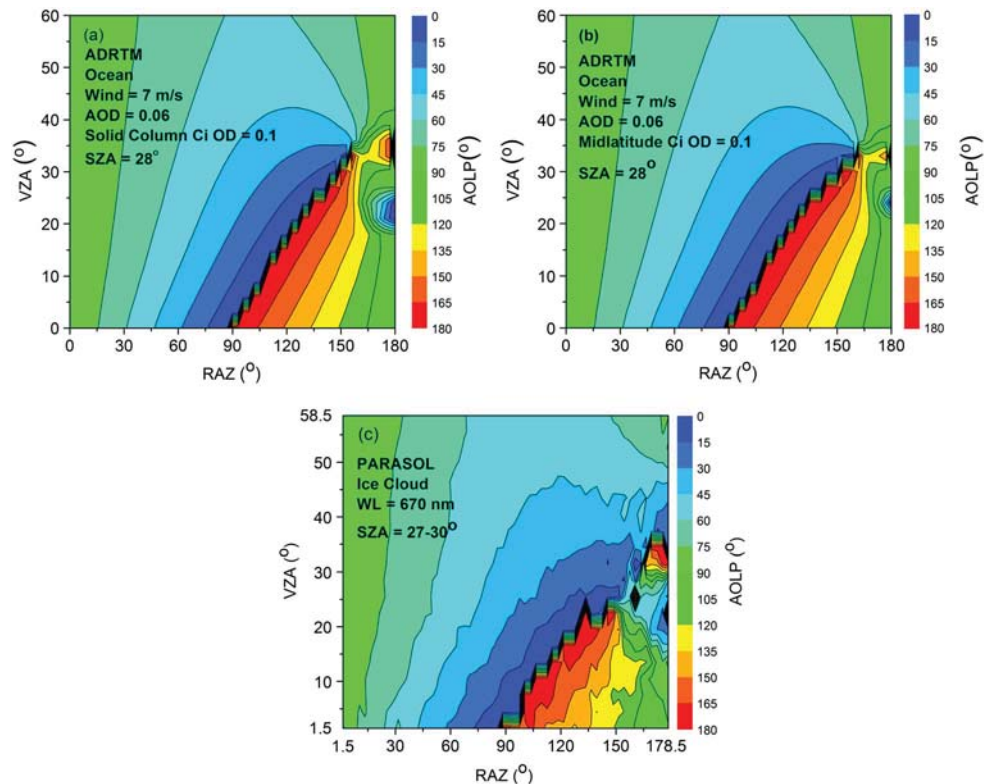
Figure 3. The AOLP at 670 nm as a function of VZA and RAZ from (a) the ADRTM for thin cirrus (Ci) composed of solid hexagonal ice columns, (b) the ADRTM for thin cirrus composed of a mixture of typical midlatitude ice particle shapes, and (c) the mean of 24 day PARASOL measurements for ice clouds over both ocean and land identified by the PARASOL product. In the modeling, the optical depth (OD) of the cirrus clouds is 0.1 at 670 nm, the wind speed is 7 m/s, the sea-salt AOD is 0.06, the SZA is 28°, and the U.S. standard atmosphere is used.

SZA is 28°, the ocean wind speed is 7 m/s, the sea-salt aerosols are of irregular shapes with an AOD of 0.06, and the U.S. standard atmosphere [*National Oceanic and Atmospheric Administration et al.*, 1976] is used. Note here that we only display the AOLPs over the RAZ range of 0° to 180°. The AOLPs over the RAZ range of 180° to 360° are symmetrically supplementary angles of the values over the RAZ range of 0° to 180° [*Sun and Lukashin*, 2013]. We find that the AOLPs from the PARASOL data and the model are similar except that at ~8° off the exact-backscatter direction (RAZ = ~180° and VZA = ~20° and ~36°), the PARASOL result shows two distinct features in the AOLP of the reflected solar light. At these viewing angles, the dominant backscattered electric field in the PARASOL data for clear-sky oceans rotates from parallel to perpendicular to the Earth's surface; whereas the modeled AOLPs do not show these features. We performed sensitivity studies with the ADRTM and found that ocean surface roughness due to winds and atmospheric gas or water vapor absorptions do not produce these features in the model outputs. However, this feature does appear when we incorporate a thin layer of cirrus into the atmosphere. The ADRTM simulation results of Figures 3a and 3b demonstrate that the presence of a super-thin layer of cirrus clouds can reproduce the AOLP features in Figure 2(a). In the simulation of Figure 3a, we incorporate the solid-column ice crystal shapes for the cirrus cloud, which may not be the ubiquitous ice crystal shapes in the atmosphere. Thin cirrus clouds are generally a mixture of various ice crystal shapes such as hexagonal columns, plates, droxtals, bullet rosettes, and aggregates. In the simulation of Figure 3b, we incorporate a typical size distribution and particle-shape mixture of midlatitude cirrus clouds [*Heymsfield and Platt*, 1984]. While not as sharp as the results of Figure 3a, we can see in Figure 3b that the distinct polarization-rotation features at the near-backscattering angles are still significant for clouds with an optical depth (OD) of only 0.1. These features remain visible even down to ODs of ~0.06. Our sensitivity studies on typical tropical cirrus produce similar results. Further evidence of the polarization-rotation features of ice clouds can be seen in the PARASOL data. Figure 3c shows the AOLPs from the mean of the 24 day PARASOL data for ice clouds over both ocean and land identified by the PARASOL product. These data are particularly noisy because of limited sampling of PARASOL at several viewing angles for ice clouds at the specific SZA. However, we can still see the polarization rotations above and below the exact-backscatter angle.
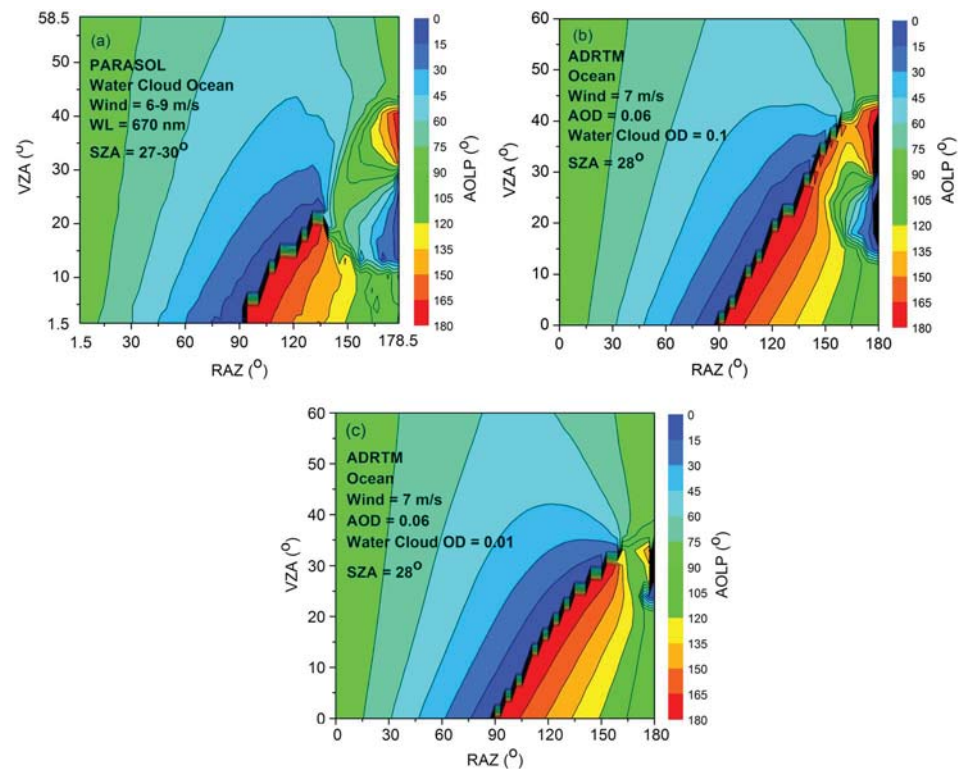
Figure 4. The AOLP at 670 nm as a function of VZA and RAZ from (a) the mean of 24 day PARASOL measurements for water clouds over oceans identified by the PARASOL product, (b) the ADRTM for water clouds with an optical depth (OD) of 0.1, and (c) the ADRTM for water clouds with an OD of 0.01 at 670 nm over oceans. In the modeling, the wind speed is 7 m/s, the sea-salt AOD is 0.06, the SZA is 28°, and the U.S. standard atmosphere is used.

One mechanism that can produce such polarization-rotation features is the optical glory. The glory is an angular region of high intensity that may extend several degrees from the exact-backscatter direction and is accompanied by a strong *p*-polarization component a few degrees from the exact-backscatter direction. This prominent *p*-polarization feature appears to be due to the internal field transmitted into the particle, and spherical droplets in water clouds can produce an especially strong glory. Figure 4a shows the AOLPs of the averaged 24 day PARASOL data of water clouds over ocean. It is clear in this figure that the glory feature is a *p*-polarized band that extends ~20° from the exact-backscatter direction (VZA ~ 28°, RAZ = 180°). Figure 4b shows ADRTM results for water clouds with an OD of 0.1, the same OD as the cirrus clouds in the simulations of Figure 3. Since the mean OD (~7.5) of water clouds from PARASOL data is much larger than 0.1, the *p*-polarized band in Figure 4a extends larger than that in Figure 4b. Also, model result in Figure 4c demonstrates that subvisual water clouds having an OD of only 0.01 still display a prominent polarization feature. This polarization feature can be suppressed when particle absorption increases and morphology becomes more irregular [*Muinonen et al.*, 2011; *Volten et al.*, 2001]. While cirrus clouds composed solely of irregularly shaped aggregated ice particles may not portray this feature [*Sun and Lukashin*, 2013], thin cirrus clouds generally contain significant quantities of simple particle shapes such as hollow or solid columns, plates, droxtals, and bullet rosettes [*Heymsfield and Platt*, 1984], especially where close to cloud top or in cold and dry regions. Additionally, since the glory prominence is dependent on particle morphology and absorption, our ADRTM simulations incorporating a dust cloud [*Volten et al.*, 2001] do not result in a noticeable glory feature in the AOLP. Such results are consistent with Hubble Space Telescope images taken during the 2003 Mars opposition that also showed *p*-polarization features, which were suggested to result from thin clouds of nucleating ice crystals. These crystals were seen at the forward edge of a prominent dust storm and were visible against a desert background, but the dust storm itself did not display such *p*-polarization features [*Shkuratov et al.*, 2005]. This demonstrates that polarization-based detection of super-thin clouds can be used over different terrain types and can differentiate such clouds from dust.

In summary, the angle of linear polarization (AOLP) of scattered sunlight observed in two distinct angular regions near the exact-backscatter direction rotates from an angle parallel to the Earth's surface to perpendicular

to the Earth's surface when cloud particles are present in the atmosphere. A sensitivity study demonstrates that the polarization-angle feature of background aerosols is not prominent enough to overcome the background polarization; however, this feature is detectable in water clouds having an optical depth of only ~0.01 and in ice clouds having an optical depth of only ~0.06, when the solar zenith angle (SZA) is not much larger than ~40° over a strong polarization background such as oceans. When over weak polarization land, the SZA can be even larger. Since most super-thin clouds are over the tropical and midlatitude regions [*Sun et al.*, 2011a, 2011b], this limit of SZA will not affect the detection of most super-thin clouds using the polarization-rotation features. Coupling this method with the total radiance measurements at a wavelength of 1.38 μm would enhance the detection of super-thin clouds and thus can significantly improve retrieval of aerosol, water vapor or other gases, and surface temperature from satellite data.

References

Ackerman, S. A., K. I. Strabala, W. P. Menzel, R. A. Frey, C. C. Moeller, and L. E. Gumley (1998), Discriminating clear sky from clouds with MODIS, *J. Geophys. Res.*, *103*, 32,141–32,157, doi:10.1029/1998JD200032.

Ackerman, S. A., R. E. Holz, R. Frey, E. W. Eloranta, B. C. Maddux, and M. McGill (2008), Cloud detection with MODIS. Part II: Validation, *J. Atmos. Oceanic Technol.*, *25*, 1073–1086, doi:10.1175/2007JTECHA1053.1.

Christi, M. J., and G. L. Stephens (2004), Retrieving profiles of atmospheric CO_2 in clear sky and in the presence of thin cloud using spectroscopy from the near and thermal infrared: A preliminary case study, *J. Geophys. Res.*, *109*, D04316, doi:10.1029/2003JD004058.

Deschamps, P. Y., F.-M. Breon, M. Leroy, A. Podaire, A. Bricaud, J.-C. Buriez, and G. Seze (1994), The POLDER mission: Instrument characteristics and scientific objectives, *IEEE Trans. Geosci. Remote Sens.*, *32*, 598–615.

Gao, B. C., and Y. J. Kaufman (1995), Selection of 1.375-μm MODIS channel for remote sensing of cirrus clouds and stratospheric aerosols from space, *J. Atmos. Sci.*, *52*, 4231–4237.

Heymsfield, A. J., and C. M. R. Platt (1984), A parameterization of the particle size spectrum of ice clouds in terms of the ambient temperature and the ice water content, *J. Atmos. Sci.*, *41*, 846–855.

McFarquhar, G. M., A. J. Heymsfield, J. Spinhirne, and B. Hart (2000), Thin and subvisual tropopause tropical cirrus: Observations and radiative impacts, *J. Atmos. Sci.*, *57*, 1841–1853.

Mishchenko, M. I., B. Cairns, J. E. Hansen, L. D. Travis, G. Kopp, C. F. Schueler, B. A. Fafaul, R. J. Hooker, H. B. Maring, and T. Itchkawich (2007), Accurate monitoring of terrestrial aerosols and total solar irradiance: Introducing the Glory mission, *Bull. Am. Meteorol. Soc.*, *88*, 677–691.

Muinonen, K., J. Tyynelä, E. Zubko, H. Lindqvist, A. Penttilä, and G. Videen (2011), Polarization of light backscattered by small particles, *J. Quant. Spectrosc. Radiat. Transfer*, *112*, 2193–2212.

National Oceanic and Atmospheric Administration, National Aeronautics and Space Administration, and United States Air Force (1976), *U.S. Standard Atmosphere*, NOAA-S/T 76–1562.

Omar, A. H., D. M. Winker, J. L. Tackett, D. M. Giles, J. Kar, Z. Liu, M. A. Vaughan, K. A. Powell, and C. R. Trepte (2013), CALIOP and AERONET aerosol optical depth comparisons: One size fits none, *J. Geophys. Res. Atmos.*, *118*, 4748–4766, doi:10.1002/jgrd.50330.

Roskovensky, J. K., and K. N. Liou (2003), Detection of thin cirrus from 1.38 μm/0.65 μm reflectance ratio combined with 8.6–11 μm brightness temperature difference, *Geophys. Res. Lett.*, *30*(19), 1985, doi:10.1029/2003GL018135.

Sassen, K. C., and S. A. Benson (2001), Midlatitude cirrus cloud climatology from the facility for atmospheric remote sensing. Part II: Microphysical properties derived from lidar depolarization, *J. Atmos. Sci.*, *58*, 2103–2112.

Shkuratov, Y., M. Kreslavsky, V. Kaydash, G. Videen, J. Bell III, M. Wolff, M. Hubbard, K. Noll, and A. Lubenow (2005), Hubble space telescope imaging polarimetry of Mars during the 2003 opposition, *Icarus*, *176*, 1–11, doi:10.1016/j.icarus.2005.01.009.

Sun, W., and C. Lukashin (2013), Modeling polarized solar radiation from ocean–atmosphere system for CLARREO inter-calibration applications, *Atmos. Chem. Phys.*, *13*, 10,303–10,324, doi:10.5194/acp-13-10303-2103.

Sun, W., B. Lin, Y. Hu, C. Lukashin, S. Kato, and Z. Liu (2011a), On the consistency of CERES longwave flux and AIRS temperature and humidity profiles, *J. Geophys. Res.*, *116*, D17101, doi:10.1029/2011JD016153.

Sun, W., G. Videen, S. Kato, B. Lin, C. Lukashin, and Y. Hu (2011b), A study of subvisual clouds and their radiation effect with a synergy of CERES, MODIS, CALIPSO, and AIRS data, *J. Geophys. Res.*, *116*, D22207, doi:10.1029/2011JD016422.

Volten, H., O. Muñoz, E. Rol, J. F. de Haan, W. Vassen, J. W. Hovenier, K. Muinonen, and T. Nousiainen (2001), Scattering matrices of mineral aerosol particles at 441.6 and 632.8 nm, *J. Geophys. Res.*, *106*, 17,375–17,401.

Wielicki, B. A., et al. (2013), Climate absolute radiance and refractivity observatory (CLARREO): Achieving climate change absolute accuracy in orbit, *Bull. Am. Meteorol. Soc.*, *94*, 1519–1539, doi:10.1175/BAMS-D-12-00149.1.

Winker, D. M., W. H. Hunt, and M. J. McGill (2007), Initial performance assessment of CALIOP, *Geophys. Res. Lett.*, *34*, L19803, doi:10.1029/2007GL030135.

Wylie, D. P., and W. P. Menzel (1999), Eight years of high cloud statistics using HIRS, *J. Clim.*, *12*, 170–184.

Wylie, D. P., P. Piironen, W. Wolf, and E. Eloranta (1995), Understanding satellite cirrus cloud climatologies with calibrated lidar optical depths, *J. Atmos. Sci.*, *52*, 4327–4343.